Protonation and Dehydration Reactions of the $Mn_4O_4L_6$ Cubane and Synthesis and Crystal Structure of the Oxidized Cubane $[Mn_4O_4L_6]^+$: A Model for the Photosynthetic Water Oxidizing Complex

Wolfgang F. Ruettinger, Douglas M. Ho, and G. Charles Dismukes*

Hoyt Laboratory, Chemistry Department, Princeton University, Princeton, New Jersey 08544

Received September 24, 1998

Synthesis of multinuclear manganese-oxo clusters is of current interest for applications to molecular magnets,[1] oxidation catalysis,[2] and bioinorganic chemistry in the area of photosynthetic water oxidation.[3−7] The inorganic core of the photosynthetic water oxidase (WOC) is comprised of a cluster of composition Mn_4O_x-Ca_1Cl_y, in which only the stoichiometry of Mn and Ca are well established.[8,9] It can be photooxidized by the photosystem II (PSII) reaction center to produce five oxidation states, differing by one electron each and designated S_0, S_1, ..., S_4. Consequently, comparisons to Mn-oxo complexes have played a key role in suggesting possible core types such as the dimer-of-dimers[8b,10] $(Mn_2O_2)O(Mn_2O_2)^{n+}$, trigonal[11a] $Mn_4O_3X^{n+}$, distorted cubane[3b] $Mn_4O_4^{n+}$, adamantane[3a,4a] $Mn_4O_6^{n+}$, and butterfly[3b] $Mn_4O_2^{n+}$.

Herein we report the synthesis and crystal structure of the $Mn_4O_4^{7+}$ cubane core cluster compound $[Mn_4O_4L_6]^+$ (**1**$^+$), obtained by an unusual dehydration/oxygenation route from $Mn_4O_4L_6$ (**1**), L = diphenylphosphinato = $Ph_2PO_2^-$. **1** and **1**$^+$ contain the first examples of the $Mn_4O_4^{6+/7+}$ cubane core and thus serve as important models for comparison to the S_3 (or S_1) and S_4 (or S_2) oxidation state of the WOC, respectively.

Complex **1** reacts with triflic acid, CF_3SO_3H (HOTf), or trimethylsilyltriflate, $(Me_3Si)CF_3SO_3$ (Me_3SiOTf), in the presence of HOTf and oxygen (vide infra) to form $[Mn_4O_4L_6]OTf{\cdot}CH_3CN$ (**1**$^+$**OTf**$^-$), which was isolated in ∼80% yield from a reaction mixture containing **1** + 2Me_3SiOTf + 2HOTf.[15]

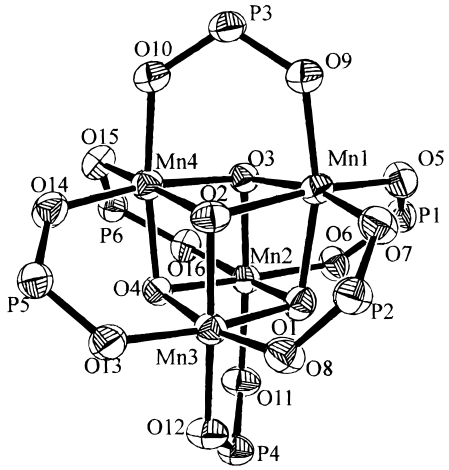

Figure 1. X-ray crystal structure (ORTEP plot with 50% probability level) of **1**$^+$**OTf**$^-$ (phenyls and counterion omitted for clarity). Selected bond lengths (Å) and angles (deg): Mn(1)−Mn(4) 2.9038(4); Mn(1)−Mn(2) 2.9826(4); Mn(1)−Mn(3) 2.9126(4); Mn(2)−Mn(4) 2.8341(4); Mn(3)−Mn(4) 2.8588(4); Mn(2)−Mn(3) 2.8377(4); Mn(1)−O(1) 2.049-(2); Mn(1)−O(2) 1.9233(14); Mn(1)−O(3) 2.040(2); Mn(2)−O(1) 1.8923-(14); Mn(2)−O(3) 1.905(2); Mn(2)−O(4) 1.9151(14); O(1)−Mn(1)−O(2) 79.35(6); O(1)−Mn(1)−O(3) 77.58(6); O(1)−Mn(2)−O(3) 84.84(7).

The crystal structure of the inner core of **1**$^+$**OTf**$^-{\cdot}CH_3CN$[14] is shown in Figure 1. The cubane cluster shows a significant trigonal distortion from tetrahedral symmetry compared to **1**, creating a trigonal pyramidal Mn_4 core with shorter Mn_{2-4}−O and longer Mn_1(apical)−Mn_{2-4}(base) bond lengths vs **1**. The mean of the three Mn_1(apical)−Mn_{2-4}(base) distances in **1**$^+$**OTf**$^-$ is 2.933 Å vs 2.844 Å for the three $Mn_{2,3}$(base)−$Mn_{3,4}$(base) vectors. The short Mn−Mn distances are 0.08−0.14 Å shorter than found in **1** and 0.2−0.1 Å longer than in typical dinuclear $[Mn_2O_2]^{3+/4+}$ cores.[12] The Mn−O distances reveal elongation around Mn_1 (avg. 2.004 Å) vs Mn_{2-4}−O(oxo) (avg. 1.8948 Å) and 1.952 Å for the Mn−O(oxo) in **1**. Also, the narrower O−Mn−O angles around Mn_1 (77.58−79.35°) vs Mn_{2-4} (82.13−84.8°) indicate a trigonally

(1) (a) Aubin, S. M. J.; Dilley, N. R.; Pardi, L.; Krzystek, J.; Wemple, M. W.; Brunel, L.-C.; Maple, M. B.; Christou, G.; Hendrickson, D. N. *J. Am. Chem. Soc.* **1998**, *120*, 4991−5004. (b) Aubin, S. M. J.; Wemple, M. W.; Adams, D. M.; Tsai, H.-L.; Christou, G.; Hendrickson, D. N. *J. Am. Chem. Soc.* **1996**, *118*, 7746−7754.
(2) Gardner, K. A.; Mayer, J. A. *Science* **1995**, *269*, 1849−1851.
(3) (a) Brudvig, G. W.; Crabtree, R. H. *Proc. Natl. Acad. Sci. U.S.A.* **1986**, *83*, 4586−4588. (b) Vincent, J. B.; Christou, G. *Inorg. Chim. Acta* **1987**, *136*, L41−L43.
(4) (a) Wieghardt, K. *Angew. Chem., Int. Ed. Engl.* **1989**, *28*, 1153−1172. (b) Wieghardt, K. *Angew. Chem., Int. Ed. Engl.* **1994**, *33*, 725−726.
(5) Christou, G. *Acc. Chem. Res.* **1989**, *22*, 328−335.
(6) (a) Armstrong, W. In *Manganese Redox Enzymes*; Pecoraro, V. L., Ed.; VCH: New York, 1992; pp 261−286. (b) Pecoraro, V. L.; Baldwin, M. J.; Gelasco, A. *Chem. Rev.* **1994**, *94*, 807−826. (c) Watkinson, M.; Whiting, A.; McAuliffe, C. A. *J. Chem. Soc., Chem. Commun.* **1994**, 2141−2142.
(7) Ruettinger, W. F.; Dismukes, G. C. *Chem. Rev.* **1997**, 97, 1−23.
(8) (a) Debus, R. J. *Biochim. Biophys. Acta* **1992**, *1102*, 269−352. (b) Yachandra, V. K.; Sauer, K.; Klein, M. P. *Chem. Rev.* **1996**, *96*, 2927−2950.
(9) (a) Zaltsman, L.; Ananyev, G.; Bruntrager, E.; Dismukes, G. C. *Biochemistry* **1997**, *36*, 8914−8922. (b) Ananyev, G. M.; Dismukes, G. C. *Biochemistry* **1997**, *36*, 11342−11350.
(10) Kirk, M. L.; Chan, M. K.; Armstrong, W. H.; Solomon, E. I. *J. Am. Chem. Soc.* **1992**, *114*, 10432−10440.
(11) (a) Wang, S.; Tsai, H.-L.; Hagen, K. S.; Hendrickson, D. N.; Christou, G. *J. Am. Chem. Soc.* **1994**, *116*, 8376−8377. (b) Wang, S.; Folting, K.; Streib, W. E.; Schmitt, E. A.; McCusker, J. K.; Hendrickson, D. N.; Christou, G. *Angew. Chem., Int. Ed. Engl.* **1991**, *30*, 305−306. (c) Wang, S.; Tsai, H.-L.; Streib, W. E.; Christou, G.; Hendrickson, D. N. *J. Chem. Soc., Chem. Commun.* **1992**, 1427−1430. (d) Aromi, G.; Wemple, M. W.; Aubin, S. J.; Folting, K.; Hendrickson, D. N.; Christou, G. *J. Am. Chem. Soc.* **1998**, *120*, 5850−5851.
(12) Manchandra, R.; Brudvig, G. W.; Crabtree, R. H. *Coord. Chem. Rev.* **1995**, *144*, 1−38.
(13) (a) Ruettinger, W.; Campana, C.; Dismukes, G. C. *J. Am. Chem. Soc.* **1997**, *119*, 6670−6671. (b) Zheng, M.; Dismukes, G. C. *Inorg. Chem.* **1996**, *35*, 3307−3319.
(14) Crystals were grown by slow evaporation of a reaction mixture containing 0.3 mM **1** in CH_2Cl_2 and 0.6 mM Me_3SiOTf and HOTf (as 10 mM solutions in CH_3CN). A dark brown prism (0.55 × 0.25 × 0.20 mm) was mounted on a glass fiber. Data collection was done with a ENRAF NONIUS Kappa CCD system equipped with a molybdenum-target X-ray tube. A total of 84 775 reflections were measured ($2.2 < \Theta < 30.03$), of which 22 301 were independent ($R_{int} = 0.0380$). Refinement of the structure in the $P\bar{1}$ space group was done by full-matrix least-squares fitting on F^2 for all reflections except for 8 with very negative F^2 and converged at $R_1 = 4.03\%$. Crystal data for **1**$^+$**OTf**$^-$: triclinic $P\bar{1}$; a = 13.8831(1) Å, b = 16.7261(2) Å, c = 18.7014(2) Å, α = 110.2338(4)°, β = 97.9111(6)°, γ = 102.5313(6)°; $Z = 2$; V = 3868.88(7) Å^3; d(calc) = 1.525 g cm^{-3}; T = 298 K. Tables of atomic coordinates and anisotropic displacement factors and ORTEP drawings of the unit cell can be found in the Supporting Information.
(15) See the Supporting Information.

10.1021/ic981145y CCC: $18.00
Published on Web 02/26/1999

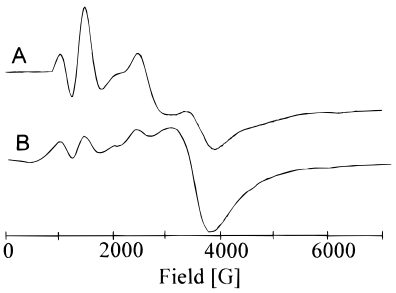

Figure 2. X-band EPR spectra (9.42 GHz) of (A) 0.5 mM $\mathbf{1}^{+}\mathbf{OTf}^{-}$ in CH_2Cl_2 frozen solution and (B) electrochemically oxidized ($E = 1.4$ V vs Ag/Ag^{+}, Pt electrode) solution of 0.3 mM **1** in CH_2Cl_2/100 mM TBAP. Measurement conditions: Bruker ESP300 spectrometer with Oxford 900 cryostat and TE102 cavity; $T = 7$ K; mod. freq 100 kHz; mod. amp 20 G; MW power 20 mW.

extended C_{3v} distortion. The coordinates are consistent with assignment of Mn_1 as Mn(III) and $Mn_{2,3,4}$ as Mn(IV). No obvious tetragonal elongation or compression of the Mn−O bonds is observed for Mn(III) in the crystal, in contrast with the carboxylato-bridged trigonally distorted cubanes with the $[Mn_4O_3X]^{6+}$ core (μ_3-X = F^-, Cl^-, Br^-, OH^-),[11] where axial Jahn−Teller elongations are observed for the three Mn(III) ions.

Unlike **1**, $\mathbf{1}^{+}\mathbf{OTf}^{-}$ has a paramagnetic ground state and solutions exhibit intense EPR spectra, as shown in Figure 2A. The signal intensity obeys the Curie law between 7 and 29 K with zero-field splitting and no resolved ^{55}Mn hyperfine structure, indicating an odd-spin ground state ($S \geq 3/2$), possibly a high-spin ground state analogous to $[Mn_4O_6Cl]^{6+}$ complexes in the III,IV oxidation state.[1a] Electrochemical oxidation of **1** at a platinum electrode ($E_{1/2} = 1.4$ V vs NHE, Figure S3)[13a] also produces $\mathbf{1}^{+}$, as seen by its EPR signal in Figure 2B. An additional species forms under electrolysis which exhibits a 400 G broad signal at $g = 2$, presumed to arise from a Mn(II) decomposition product. Other oxidants such as $NOBF_4$ or Cl_2 also oxidize **1** to $\mathbf{1}^{+}$, as evidenced by EPR spectra, but the product always contains contamination from other species, in particular Mn(II). **1** can be recovered quantitatively from solutions of $\mathbf{1}^{+}\mathbf{OTf}^{-}$ by addition of reductants such as triethylamine or many common solvents such as MeOH, EtOH, DMF, and DMSO. NMR reveals that the one-electron reduction of $\mathbf{1}^{+}$ to **1** by 1 equiv of Et_3N (Figure S7) proceeds via an intermediate of lower symmetry than either $\mathbf{1}^{+}$ or **1**. The identity of the intermediate is unknown, but might involve formation of the triply bridging amine−oxide, Mn_4O_3-(μ_3-$ONEt_3$)L_6. Such an intermediate would be relevant to possible water oxidation schemes involving addition of water or hydroxide to a μ_3-oxo.[7] These data establish that formation of $\mathbf{1}^{+}\mathbf{OTf}^{-}$ by acidification of **1** in air involves one-electron oxidation rather than protonation of **1**.

UV−vis (Figure S2) and NMR (Figure S6) titrations in air show that ∼2 equiv of HOTf is needed for conversion of **1** to $\mathbf{1}^{+}\mathbf{OTf}^{-}$ with ≥84% yield (NMR integration). The near quantitative yield of $\mathbf{1}^{+}$ indicates that it could not form entirely by disproportionation of **1**. A requirement for oxygen in the formation of $\mathbf{1}^{+}\mathbf{OTf}^{-}$ from **1** + HOTF was established by UV−vis titrations under anaerobic conditions (Figures S2b, S4, S5).

The formation of $\mathbf{1}^{+}$ by oxidation of **1** can also be initiated by addition of 2 equiv of Me_3SiOTf, but proceeds to only 50% conversion of **1** independent of the presence of oxygen and yields 1 equiv of $(Me_3Si)_2O$, as established by NMR and UV−vis (Figures S8, 9, 12). Subsequent addition of 2 equiv of HOTf leads to complete conversion to $\mathbf{1}^{+}$ under aerobic conditions (Figure S9). ESI−MS (positive ions) spectra of reaction mixtures show the initial formation of the species $[Mn_4O_3L_6]^{+}$ (m/z 1570) independent of whether the reagent is HOTf or Me_3SiOTf (Figure S11).

The observed reactions of **1** can be explained by the following equations (L = $Ph_2PO_2^-$; R = H, Me_3Si):

$$\text{(A)}\quad Mn_4O_4L_6\ (\mathbf{1}) + ROTf \rightarrow Mn_4O_3(OR)L_6^{+} + OTf^{-}$$

$$\text{(B)}\quad Mn_4O_3(OR)L_6^{+} + \mathbf{1} \rightarrow Mn_4O_3(OR)L_6 + \mathbf{1}^{+}$$

$$\text{(C)}\quad Mn_4O_3(OR)L_6 + ROTf \rightarrow R_2O + OTf^{-} + Mn_4O_3L_6^{+}$$

$$\text{(D)}\quad Mn_4O_3L_6^{+} + {}^1/_2O_2 \rightarrow Mn_4O_4L_6^{+}\ (\mathbf{1}^{+})$$

Initially a proton (R = H) or a trimethylsilyl cation (R = Me_3-Si) binds to **1** (A), yielding $[Mn_4O_3(OR)L_6]^{+}$ and thus converting it to a stronger oxidant.[16] We propose that this species oxidizes unreacted **1** to $\mathbf{1}^{+}$ (B), thus limiting the yield to 50% for R = Me_3Si in the absence of HOTf. The resulting one-electron reduced species, $Mn_4O_3(OR)L_6$, continues to react with ROTf to remove one oxide bridge completely as R_2O (C), forming the deoxygenated intermediate $[Mn_4O_3L_6]^{+}$, which is detected by ESI−MS (m/z 1570) and which, in turn, is oxidized by O_2 in the presence of protons (from HOTf) to form $\mathbf{1}^{+}$ (D) for a total theoretical yield of 100%.

The isolation of $\mathbf{1}^{+}\mathbf{OTf}^{-}$ extends the known Mn_4O_4 cubane core type to include the Mn_4(III,3IV) oxidation state, a possible model for the S_2 (ref 8b) or S_4 (ref 13b) oxidation states of the WOC. The assignment of Mn oxidation states in the WOC is an unresolved issue, with different conclusions reached from Mn XANES data[8b] vs ^{55}Mn EPR data.[13b] EPR spectral data of the "cubanes" $[Mn_4O_4L_6]^{-/0/+}$ (ref 17), however, support the EPR-derived assignment for the Mn oxidation states of the S_2 state as Mn_4(3III,IV).

The isolation of $\mathbf{1}^{+}\mathbf{OTf}^{-}$, the highest oxidation potential Mn-oxo cluster yet synthesized, will enable exploration of new oxidation chemistry with organic and inorganic precursors, as well as possible pathways for O_2 production from water that are related to the mechanism of photosynthetic O_2 evolution.

Acknowledgment. The research was supported by the National Institutes of Health, GM39932. W.R. acknowledges fellowship support from an NIH training grant in Molecular Biophysics and a Patchett Summer Fellowship.

Supporting Information Available: UV−vis, ^{1}H NMR, GC−MS, and mass spectra of the reactions of **1** with HOTf and $(CH_3)_3SiOTf$; ORTEP drawing of the unit cell and asymmetric unit of $\mathbf{1}^{+}\mathbf{OTf}^{-}\cdot CH_3CN$ with numbering scheme; tables of atomic coordinates, bond lengths and angles, and anisotropic displacement factors for $\mathbf{1}^{+}\mathbf{OTf}^{-}$. This material is available free of charge via the Internet at http://pubs.acs.org.

IC981145Y

(16) (a) Thorp, H. H.; Sarneski, J. E.; Brudvig, G. W.; Crabtree, R. H. *J. Am. Chem. Soc.* **1989**, *111*, 9249−9250. (b) Cooper, S. R.; Calvin, M. *J. Am. Chem. Soc.* **1977**, *99*, 6623−6630. (c) Baldwin, M. J.; Pecoraro, V. L. *J. Am. Chem. Soc.* **1996**, *118*, 11325−11326.

(17) Dismukes, G. C.; Ruettinger, W. F.; Boelrijk, A. E.; Ho, D. Structure of the Mn_4Ca_1 Core of the PSII Water Oxidizing Complex and the Mn_4O_4-Cubane/Mn_4O_2-Butterfly Model Complexes. In *Photosynthesis: Mechanisms and Effects*; Garab, G., Ed.; Kluwer Academic: Dordrecht, 1998; pp 1259−1266.